Supplementary Information

Unique calibration of passive air sampling for field monitoring of PAHs with polyethylene thin films across seasons and locations

Jana Meierdierks [a*], Christiane Zarfl [a], Barbara Beckingham [b], Peter Grathwohl [a]

[a] *Center for Applied Geosciences, University of Tübingen, Tübingen, Germany*

[b] *Department of Geology and Environmental Geosciences, College of Charleston, Charleston SC, USA*

S.1. Sampling sites

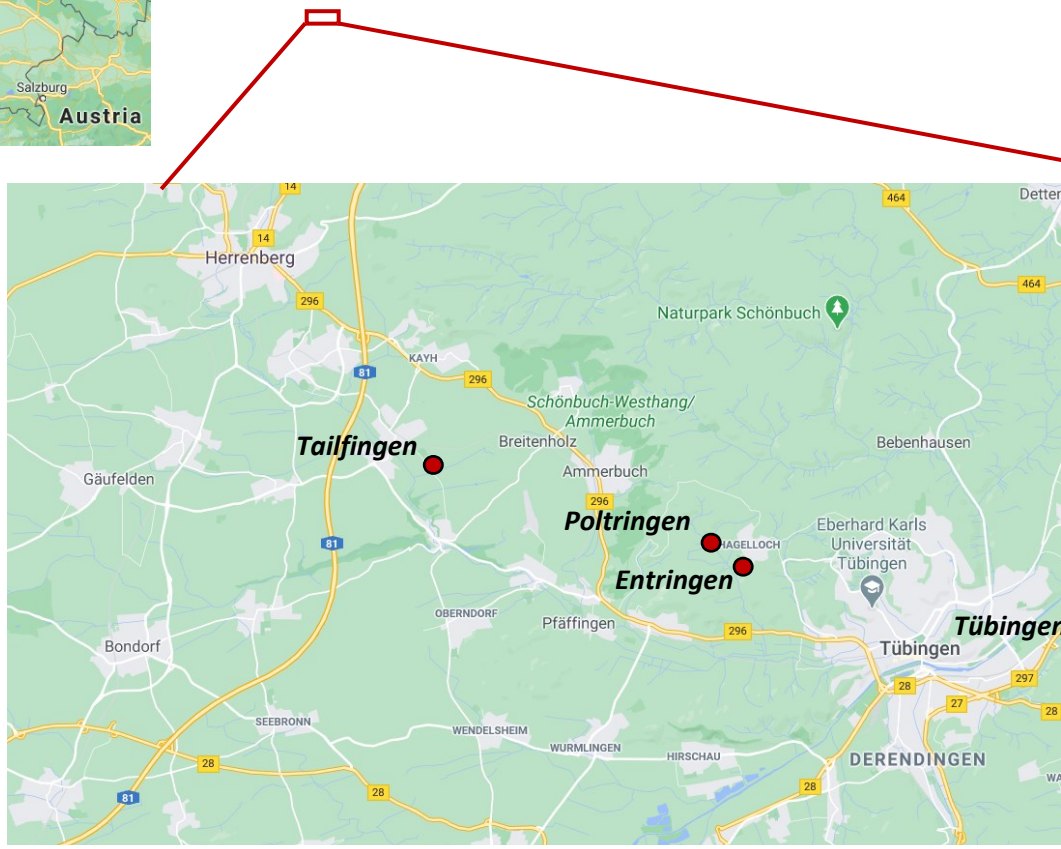

Figure.S 1: Top: Map of Germany with the study region marked in red. Bottom: Study sites Entringen, Poltringen and Tailfingen in red. Both maps were downloaded from Google.maps (11.12.20).

S.2. Set

Figure.S 2: Sampler set-up in the field. Left: Aluminium box with 55 x 55 x 10 cm (l, w, h), fixed in 1.2 m height above ground. Right: View into the box cover, which is open at the bottom. PE sheets hanging within the box cover.

S.3. Test on photodegradation on the sampler

S.3.1. Preliminary test on the sampling design

The monitoring covered two weeks between 30th of September and 14th of October in 2015 with specific sampling times after 12 and 24 hours as well as 3, 6 and 13 days; samples were always taken in duplicate for each setting. Black and transparent sheets were spiked separately with Ant-D10 as PRC before deployment. In the field an aluminium cover at 1.2 m height was used to protect sheets against the influence of wind, rain and direct sunlight, while uncovered sheets were attached to a cord, spanned right beside the cover at about 1.6 m height. The different PE sheets varied additionally in their thickness with 30 µm (transparent PE) and 80 µm (black PE).

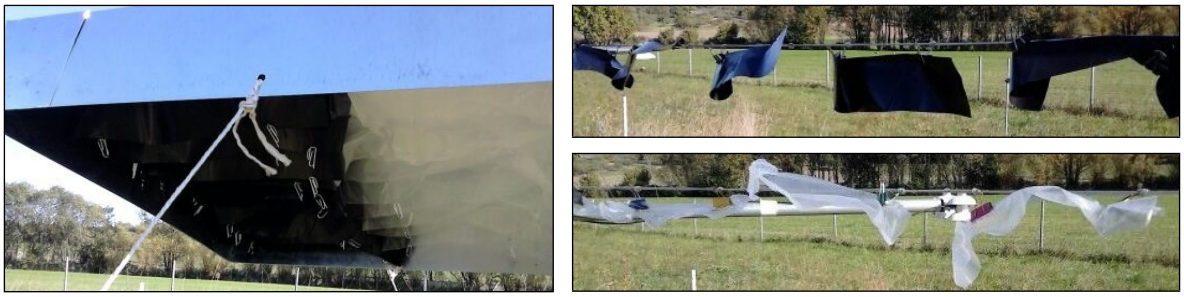

Figure.S 3: Different sampling set-ups in the field (Entringen): Left: Transparent and black PE sheets hanging within the aluminium box cover. Right: Black (top) and transparent (bottom) sheets hanging freely without protection from wind, sunlight etc..

Figure.S 4 shows a good fit for the measured and the modelled loss of Ant-D_{10} from PE for each of the individual settings and sheets. The release-curves of Ant-D10 from PE show a very comparable trend for all four designs – only the initial concentrations on PE vary significantly (this was due to a spiking solution without 20% organic solvent). Based on these loss curves, air side boundary layers (δ_g) were fitted and respective rate constants for Ant-D10 were calculated based on the fitted δ_g, as listed in ***Table.S 1***. Higher loss rates were measured for the uncovered samplers with 0.3-0.37 [day^{-1}] compared to 0.17-0.25 [day^{-1}] for the covered sheets. As expected, the thickness of the air -side boundary layer of the covered set-up is approx. two times larger than in the uncovered set-up. The resulting atmospheric concentrations calculated for the four representative PAHs are also listed in ***Table.S 1***. In all settings similar concentration were determined for Phe indicating no major influence of photodegradation of PRC or target compound in PE. For the other compounds, differences of a factor of two or more were observed with no clear tendency of covered vs. open or black vs. transparent.

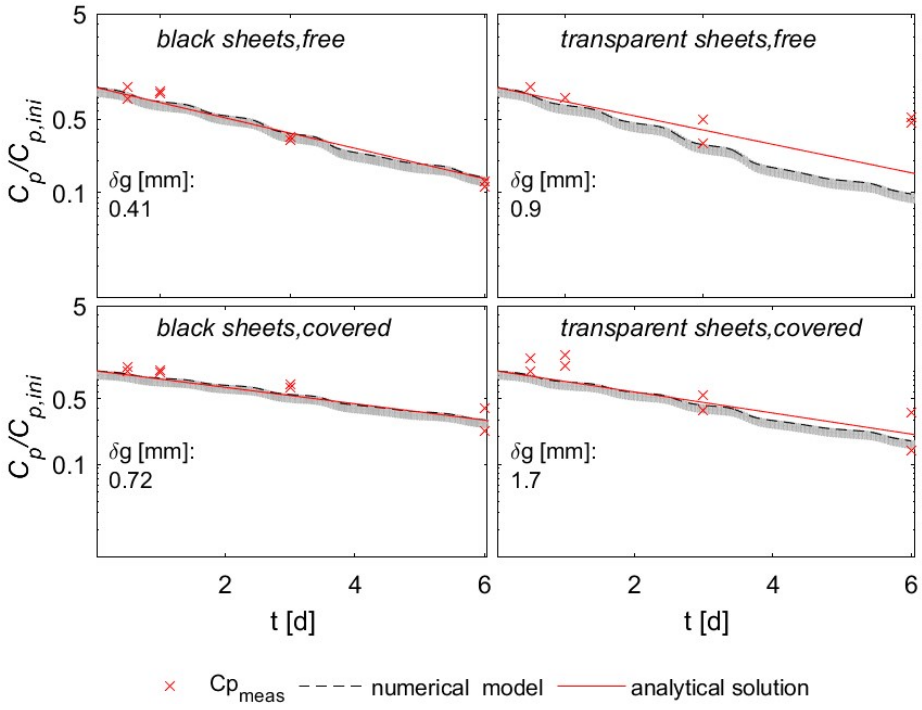

Figure.S 4: Measured (red crosses) and modelled (dashed line) loss of the PRC from PE sheets, normalized to the initial PRC-concentration on PE. The different sampling set-ups in the field are compared with transparent versus black sheets as well as covered and uncovered. The shaded grey area illustrates a standard deviation of 10 % and the red line shows the analytical solution.

Table.S 1: Loss rate constant k_e [day^{-1}] (calculated with fitted δ_g) and fitted atmospheric concentrations [ng/m^3] of Fln, Phe, Fth and Pyr for the comparison of the different sampling set-ups in the field.

field set-up	k_e [day^{-1}]	Fln [ng/m^3]	Phe [ng/m^3]	Fth [ng/m^3]	Pyr [ng/m^3]
black, uncovered	0.3	1.7 ± 0.3	2.2 ± 0.1	0.3 ± 0.03	0.2 ± 0.04
black, covered	0.17	1.7 ± 0.1	2.2 ± 0.3	0.3 ± 0.05	0.2 ± 0.06
transparent, uncovered	0.37	3.4 ± 0.5	2.6 ± 0.4	0.1 ± 0.07	0.1 ± 0.02

transparent, covered	0.25	3 ± 0.3	3.6 ± 0.2	0.9 ± 0.05	0.4 ± 0.01

48

49

50 S.3.2. Diurnal variations

51 In order to evaluate diurnal changes in concentration we conducted a day vs. night sampling in
52 Entringen at the end of the sampling campaign in November 2017, when LMW PAHs are expected to
53 have reached dynamic equilibrium between PE and air. During this sampling campaign we added a
54 second set of samplers at 10 cm above ground (also below a cover). After a very sunny day (with 7
55 hours of sunlight) samples were taken in duplicates in both heights (4 replicates in total) right before
56 sunset. The next set of samples was taken 15 hours later, during sunrise. For most of the PAHs sunset
57 and sunrise sampling results agreed very well as shown in Figure.S 5. Only the most volatile
58 compounds (naphthalene, acenaphthene and acenaphthylene) show higher concentrations on PE
59 sampled overnight, at both heights. This observation can be explained by the rapid equilibration of
60 these compounds (within hours), changes in gaseous concentrations and the temperature sensitivity
61 of the partition coefficient. The air temperature was higher when sampling at sunset (10°C) compared
62 to sampling in the morning (2°C) leading to a lower K_{pg} and lower C_p.

63

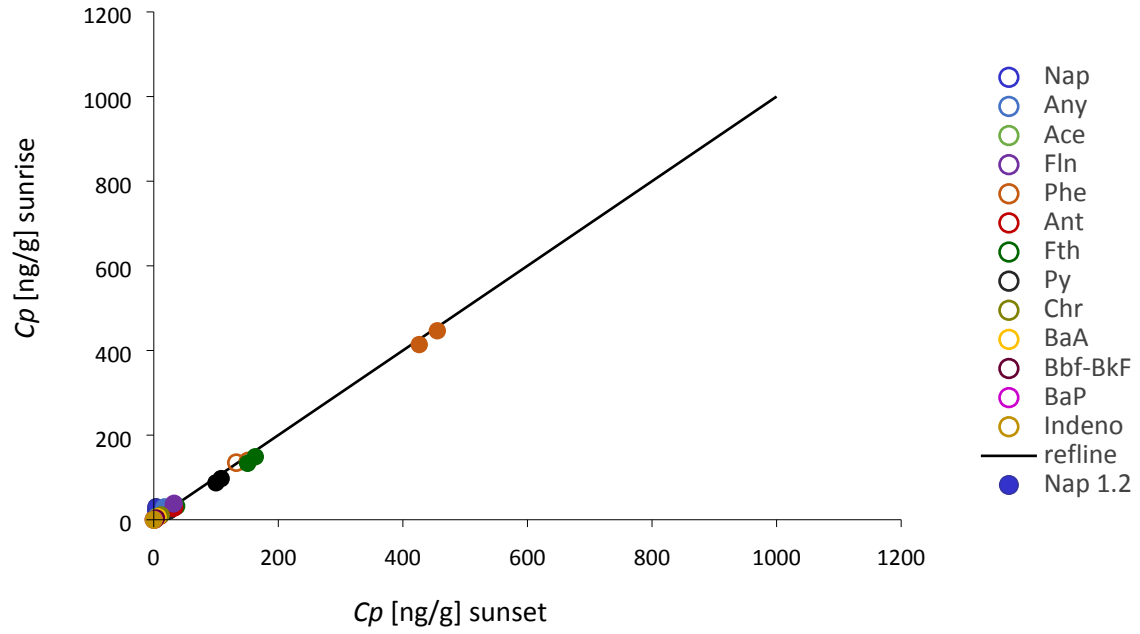

64

65 *Figure.S 5: Concentrations of 13 PAHs measured on PE after three weeks of sampling during November 2017 (here, all*
66 *compounds which exceed the limit of quantification are considered). Samples taken after a sunny (and warm) day (10 °C) are*
67 *compared to samples taken at the sunrise of the next day (2 °C); duplicate samples at 120 cm (filled symbols) and 10 cm (open*
68 *symbols) above ground, in total four replicate samples at both sampling times.*

S.3.3. Comparison of different deuterated compounds as *PRC*

During the first three sampling campaigns in our seasonal monitoring we spiked the PE sheets additionally with Pyr-D10 (following [67]). But only during May 2016 we determined a reliable change of concentrations of Pyr-D10 on PE, which is shown in Figure.S 6. As expected, the loss of Ant-D10 is faster than for Pyr-D10, and the fitted air-side boundary layer was in close agreement for both compounds with 0.6 ± 0.1 mm based on Ant-D10 and 0.3 ± 0.1 mm based on Pyr-D10.

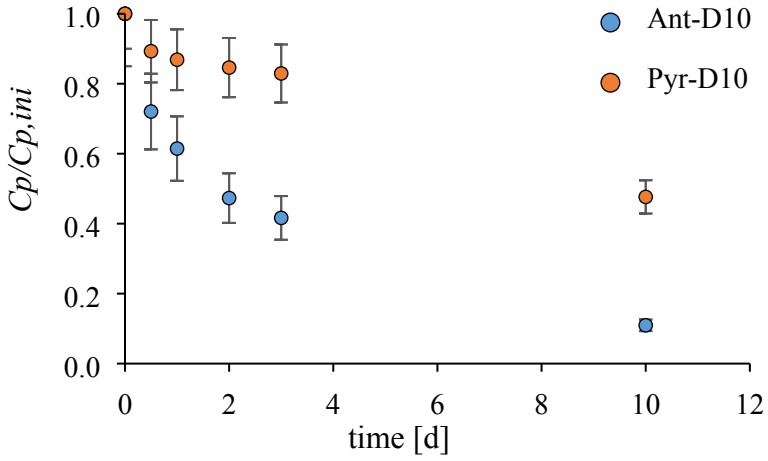

Figure.S 6: PRC-loss during May 2016, comparing Ant-D10 and Pyr-D10. Concentrations shown here are average values for the three sites and 3 replicate samples per sampling time; error bars refer to a standard deviation of 10%.

S.4. Mass transfer resistances

To check on the potential influence of the polymer-side boundary layer on the overall exchange kinetics, we use the double-film diffusion model and compare the relative thicknesses of air and polymer-side boundary layers:

$$\frac{dC_p}{dt} = -\frac{2}{\frac{d\,\delta_{poly}}{D_{poly}} + \frac{\delta_g K_{p/g}}{D_g}}\left(C_p - C_{p,eq}\right) \qquad (1.7.b)$$

Here, D_p is the diffusion coefficient [m²/sec] within the polymer, δ_p denotes the polymer-side boundary layer, which was so set to a maximum value of $d_p/2$. Diffusion coefficients in polyethylene (D_p) are about 10^6 smaller than in the gas phase (D_g) and log K_{pg} is greater than 10^6 (compounds with molecular weights larger than Naphthalene). Since δ_p is at maximum half of the thickness of the PE sheet (< 40 µm), δ_g with a thickness of I mm will control mass transfer.

S.5. Calibration of the air-side boundary layer comparing different time spans

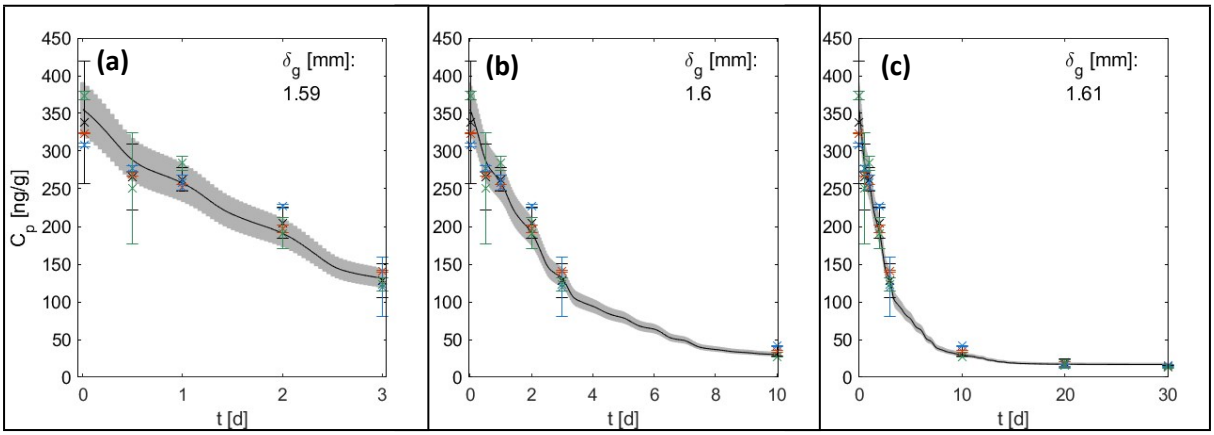

Figure.S 7: PRC-loss during August 2016 measured at each location (crosses: red – Entringen, green – Poltringen, blue – Tailfingen) over different time periods; black solid line: numerical model fit based on measurements averaging over all locations. The air-side boundary layer thickness δ_g was fitted for the average concentrations on PE, accounting for different time spans: (a) 3 days (b) 10 days (c) 30 days. Error bars refer to triplicate samples at each location and the grey area indicates the standard deviation of the predicted concentration.

S.6. Comparison of *Cg* estimated with the numerical model and the analytical solution

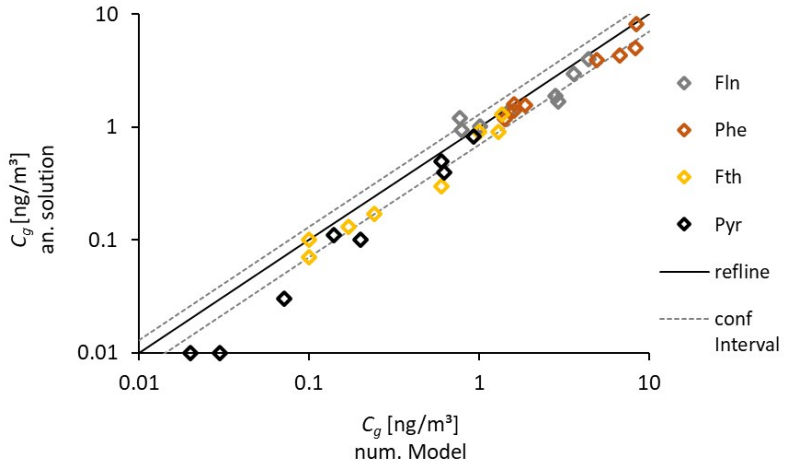

Figure.S 8: Scatter plot comparing atmospheric concentrations of the four target PAHs determined with the analytical solution (y-axes) based on Eq. 1.4 to the numerical model (x-axes) based on Eq. 1.7. This comparison accounts for all seasonal samplings during the first year of monitoring. The solid line delineates the 1:1 reference line while dashed lines refer to a confidence interval of ±30%.

S.7. Distribution pattern of the representative PAHs determined with active samplers

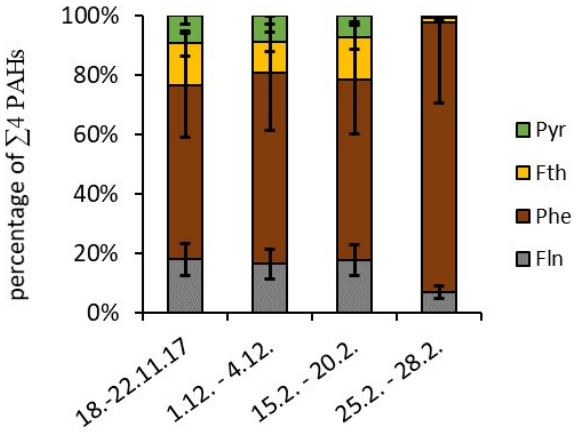

Figure.S 9: Percentage distribution of the four representative PAHs determined with active samplers. Error bars denote a standard deviation of 30%. The different pattern observed for the last sampling (25-28th of February 2018) is probably caused by the lack of particles sampled on glass fibre filters during this period.

S.8. C_g of Fln, Fth and Pyr estimated based on their ratio to Phe

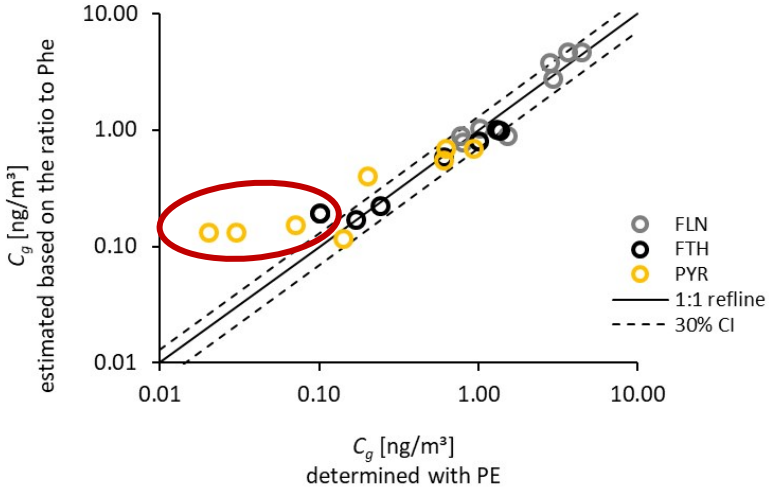

Figure.S 10: Atmospheric concentrations of Fln, Fth and Pyr for all seasons and all locations calculated from Phe and the average distribution pattern. The red circle denotes outliers of Pyr during the warm periods as well as Fth during August 2017.